Numerical modelling of reverse-density structures in soft non-Newtonian sediments

PHILIP HARRISON[1] & ALEX J. MALTMAN[2]

[1]*Department of Applied Mathematics, University of Wales, Aberystwyth, Wales SY23 3DB, UK*
[2]*Institute of Geography and Earth Sciences, University of Wales, Aberystwyth, Wales SY23 3DB, UK*

Abstract: A numerical code has been used to simulate the flow patterns in geological soft sediments that are driven by buoyancy forces resulting from reverse-density stratification. The aim was to provide a clearer understanding of the different roles of initiating conditions, inertia and rheological behaviour on the morphologies and timing of formation of natural features such as load casts and flame structures. Particular attention was paid to the cuspate form of rising intrusions that is commonly seen in nature but that has proved elusive in most earlier experiments. The numerical results demonstrate that large localised initiating perturbations and inertial influence during flow both tend to cause a decrease in the wavelength of the resulting flow pattern and can, under certain circumstances, serve to promote a cuspate morphology. The use of a relatively low viscosity Newtonian fluid as an approximation of the coarse-grained upper layer coupled with, critically, power-law behaviour in the underlying clayey layer was also found to promote a cuspate form in the rising intrusion.

Mobilization structures in geological soft sediments have long been described but the need has grown for a more quantitative understanding of their genesis (e.g. Prentice, 1961; Brodzikowsk & Van Loon 1985; Cegla *et al.* 1987). This paper reports our attempts to model the gravity driven soft sedimentary features known in geology as load casts and flame structures (Keunen 1953; Pettijohn & Potter 1964). Such structures are widely seen in rocks formed from interlayered sequences of sand-rich and clay-rich sediments, which are inferred to have had different densities at the time of deformation. The features arise by a combination of the upward growth of the lower clay-rich sediment and the downward loading of the upper sand-rich sediment (for example, see Fig. 1). Although flames are sometimes loosely referred to as dewatering structures, most analyses have regarded them as natural examples of Rayleigh-Taylor instabilities (Allen 1984; Collinson & Thompson 1987; Ronnlund 1989). These arise where one homogeneous fluid of constant density is superposed above one of lesser density. The extent to which any water loss plays a part is unclear, but Rayleigh-Taylor instability theory has proved to be a most useful basic approach to understanding these structures. For example, information is easily found on both the wavelength of the flow pattern and the rate of growth of a perturbation within a system that contains Newtonian fluids of known viscosities and densities (Ramberg 1968*a*, *b*). Although some of the principles are applicable to mobilization on a larger scale, and in materials such as salt and magma, this investigation is restricted to soft sediments.

Analytical approaches to the problem (e.g. Bio & Odé 1965; Turcotte & Schubert 1982) are limited in a number of significant ways. For example, they are all restricted to the initial stages of growth of an instability, that is until the amplitude of the perturbation reaches around only 10% of the wavelength and many natural structures are likely to have progressed well beyond this stage (Ramberg 1981; Johnson & Fletcher 1994). In addition, most considerations are restricted to the linear terms that occur in the related Navier-Stokes equations. In particular, they consider strictly Newtonian behaviour – which is not normally the case in soft sedimentary materials – and they assume non-inertial flow (e.g. Maltman 1984; Coussot & Piau 1994). The exceptions to these last two shortcomings are Biot (1963*a*, *b*), who introduced elasticity and Chandrasekhar (1955), who included inertial terms from the Navier-Stokes equations.

An alternative approach to understanding reverse-density structures is to simulate them experimentally in the laboratory. This can provide insights beyond the scope of theoretical analysis but also involves significant shortcomings. For example, simple experiments designed to model these structures using geological materials such as mud and sand (e.g. Anketell *et al.* 1970) are difficult to control because of the complex rheologies involved and the developing structures are impossible to observe in opaque sediments. Other experiments, often originally designed to model the growth of salt domes, have used simpler and more translucent fluids such as oil and syrup (Whitehead & Luther 1975; Talbot 1977) or have involved more elaborate modelling techniques such as pressure driven accelerations or centrifuges (e.g. Lewis 1950). These experiments have added

From: VAN RENSBERGEN, P., HILLIS, R.R., MALTMAN, A.J. & MORLEY, C.K. (eds) 2003. *Subsurface Sediment Mobilization.* Geological Society, London, Special Publications, **216**, 35–50. 0305-8719/03/$15

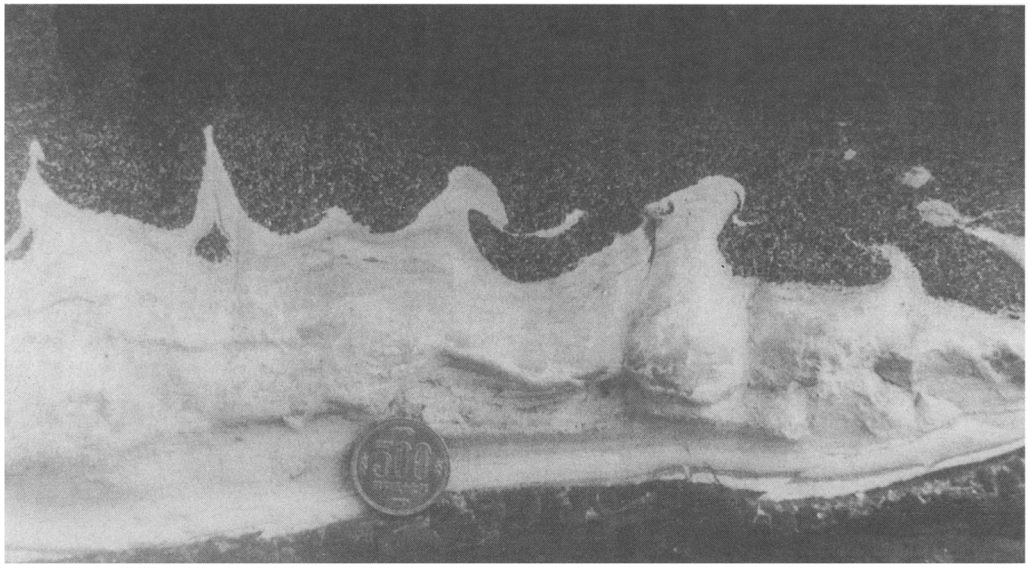

Fig. 1. Rounded load casts composed of lithified volcanic sand (upper, dark coloured layer) and cuspate flame structures (lower, pale coloured layer) in mudstone. Note the pointed, cuspate form of the flame structures, well shown at the left-hand side of the photograph. Eocene volcanogenic turbidite sequence, Boso Peninsula, Japan. Coin is approximately 2 cm in diameter.

considerably to the understanding of reverse-density structures but are limited in describing the flow behaviour of soft sediments because of their inherent differences from the geological situation.

Over the last 30 years or so, advances in computer technology have led to the rise of numerical modelling as a powerful means of predicting the behaviour of physical systems. This numerical approach (Schmeling 1988; Romer & Neugebauer 1991; Poliakov *et al.* 1993; Van Keken *et al.* 1993) has allowed many of the simplifications and limitations of the analytical and experimental analysis of Rayleigh-Taylor instabilities to be overcome. In particular, numerical simulations have provided results from stages of diapiric development far beyond the scope of analytical theory and have included factors such as depth- and temperature-dependent viscosities, syn-depositional diapiric growth, multiple layers, erosion at the surface and non-Newtonian behaviour.

We report here our attempts to use modern numerical and rheological techniques to examine the initiation and development of reverse-density structures in unlithified sediments. First, the method underlying the numerical code is summarized. All the simulations were two-dimensional and were either planar or axisymmetric. Then the use of the code to provide insights into factors that are thought to be linked with the development of naturally occurring reverse-density soft sedimentary structures, including the effects of the size and form of the initial perturbation and the possibility of inertial flow is described. Rheological experiments allowed appropriate fluid behaviours to be incorporated in the code. Once the problem was correctly stated within the program, material parameters, boundary conditions or geometry were varied in order to observe the effects of these changes on a given system. In particular, specific attention was paid to the pointed or cuspate morphology (Walton 1956; Brodzikowski *et al.* 1987) of many natural flame structures (see, for example, Fig. 1). Although this cuspate form has already been explained by second order analysis of 'mullion structure', in which sediment layers are subjected to uniform shortening or extension (Johnson & Fletcher 1994), its connection with reverse-density structures has intrigued earlier workers but has proved difficult to simulate in most experimental investigations. Dżułyński and collaborators made the most successful attempts during the 1960s (e.g. Anketell *et al.* 1970), although the precise reasons behind the cuspate form are impossible to identify from their experiments.

The numerical code

The commercially available numerical-modelling package 'Polyflow' (Polyflow s.a., Pl. de L'Université, 16, B-1348, Louvain-la-Neuve, Belgium: e-mail; support@polyflow.be) was employed, which was designed to simulate industrial

non-linear fluid flow problems (e.g. Debbaut *et al.* 1997; Yao & McKinley 1998). Polyflow is a general-purpose program that solves partial differential equations using the finite element technique and is designed for simulating flow-processes dominated by non-linear viscous flow phenomena and viscoelastic effects. It is based on the general principles of continuum mechanics together with various phenomenological and kinetic theoretical models of the rheological behaviour of fluids. The models used in this investigation were Newtonian and power-law. The program was run on a 'Dec Alpha 3000' computer.

All the simulations of this investigation incorporate an incompressible fluid condition. Using this condition we have for the Cauchy stress tensor,

$$\sigma = p\mathbf{I} + \tau \tag{1}$$

where p is the pressure, $\mathbf{I}$ is the unit tensor and τ is the extra stress tensor. The form of the extra stress tensor depends on the type of fluid; in the case of a generalised Newtonian fluid the extra stress tensor is given by

$$\tau = \eta(|\mathrm{II}|).2\mathbf{D} \tag{2}$$

where $\eta(|\mathrm{II}|)$ is the coefficient of viscosity of the fluid and for complex flows is assumed to be a function of the second invariant of the rate of deformation tensor, $2\mathbf{D}$ (Macosko 1994). The coefficient of viscosity of a Newtonian fluid is constant whereas power law behaviour is given by

$$\eta(\mathrm{II}) = K \cdot |\mathrm{II}|^{(\eta-1)/2} \tag{3}$$

which involves a consistency factor K with dimensions ($Pa.s^n$) and a power law index n.

Eqs 1 and 2 can be substituted into an equation of motion

$$\nabla . \sigma + \rho\mathbf{F} = \rho\frac{D\mathbf{v}}{Dt} \tag{4}$$

which arises from the conservation of linear momentum. Here ρ is the density of the fluid, $\mathbf{F}$ is the external body force per unit mass, $\mathbf{v}$ is the velocity vector and the operator D/Dt is the material time derivative. When considering the flow of a Newtonian fluid the substitution produces the classical Navier-Stokes equations. A similar substitution can be made based on the power law model, i.e. by incorporating Eq. (3). Upon specifying the boundary and initial conditions of the problem the resulting equations, along with the continuity equation which results from the conservation of mass of an incompressible fluid

$$\nabla \cdot \mathbf{v} = 0 \tag{5}$$

are solved by the numerical calculations.

In order to accommodate different sets of equations existing in different parts of a domain, for example due to changes in the material properties and different boundary conditions on different sections of the boundary, the concepts of sub-domains and boundary sets are used. Each sub-domain corresponds to a group of finite elements and boundary sets are groupings of finite element connectors located on the domain boundary. A well-posed time-dependent problem requires the specification of initial conditions throughout the domain along with the necessary boundary conditions. During this investigation certain boundary conditions have been used repeatedly. These include a no-slip condition

$$\mathbf{v}_n = \mathbf{v}_s = 0 \tag{6}$$

where $\mathbf{v}_n$ is the normal velocity and $\mathbf{v}_s$ is the tangential velocity, and a plane of symmetry condition

$$\mathbf{v}_n = \mathbf{f}_s = 0 \tag{7}$$

where $\mathbf{f}_s$ is the tangential force. Additionally, in certain simulations a free surface condition was imposed on the upper boundary. For this condition one requires simultaneously that the normal force $\mathbf{f}_n$, the tangential force $\mathbf{f}_s$, and the normal velocity $\mathbf{v}_n$ be prescribed. Surface tension enters in the system as a force that has the direction of the normal to the free surface

$$f_n\hat{\mathbf{n}} = \frac{\varepsilon}{R}\hat{\mathbf{n}} \tag{8}$$

where $\hat{\mathbf{n}}$ is the unit vector normal to the surface, R is the Gaussian curvature of the surface and the parameter ε is the surface tension coefficient. This normal force introduces tangential forces at both ends of the free surface

$$\mathbf{f}_s\hat{\mathbf{s}} = \varepsilon.\hat{\mathbf{s}} \tag{9}$$

where $\hat{\mathbf{s}}$ is the unit vector tangent to the free surface and directed away from the surface. Finally

$$\left(\frac{d\mathbf{x}}{dt} - \mathbf{v}\right).\hat{\mathbf{n}} = 0, \tag{10}$$

where $\mathbf{x}$ is the position of a node on the free surface. Eq. (10) is the kinematic condition for a time dependent problem and means that the free surface must follow material points in the normal direction, the tangential displacement being left arbitrary.

The final condition used in the simulations is a moving interface condition, which occurs along the intersection of two sub-domains, Ω_1 and Ω_2. This condition holds when the kinematic condition, Eq. (10), is added to the conditions

$$\mathbf{v}_1 = \mathbf{v}_2, \tag{11}$$

$$\mathbf{f}_1 = \mathbf{f}_2 \tag{12}$$

which ensures the continuity of the velocity vector and surface force over the interface.

Remeshing techniques are necessary when free

surface or moving interfaces are present. Throughout this investigation the Thompson transformation (Thompson 1985), which was designed to accommodate complex deformations in all directions of the Cartesian space, is implemented. The Galerkin method is used in choosing the shape functions for the calculations. The interpolant used for the velocity, pressure and co-ordinate fields are respectively quadratic, linear and quadratic. A first order Euler explicit-implicit predictor corrector method is used to calculate the evolution of the system in time.

Rheological behaviour of sediments

An important step in moving towards the reality of natural geological situations is to incorporate into the simulations the density and rheological behaviour of typical sediments. It is convenient to begin by considering the higher and lower density sediments separately, i.e. the rheological behaviours of the upper and lower components of a two-layer instability. The difference in densities is usually a result of the packing efficiency of the constituent particles. Muddy sediments, consisting of very fine-grained clay particles with equivalent diameter 4 microns or less, will form the less dense sediments whereas sandy sediments tend to form the denser layers. This is because the surfaces of clay particles are subject to weak but significant electrostatic forces. These forces limit the packing efficiency of the particles (Cheng 1987).

If the principles of continuum mechanics are to be used in simulating flow the system has to be treated as homogeneous, hence the particles within the fluids must be small in relation to the dimensions of the system under consideration (Anketell and Dżułyński 1968). The numerical simulations presented in the present study involve layers measuring approximately one or two centimetres thickness and so the rheological behaviours of materials containing particles with equivalent diameters no larger than 1000 microns are considered. In order to differentiate between fine and coarse-grained particles, arbitrary size limits are used in accordance with convention. Thus, coarse-grained particles are limited to sand particles measuring between 63 and 1000 microns equivalent diameter and fine-grained particles include clay and silt with equivalent diameter less than 63 microns.

These limits provide the definition of what we mean by 'fine-grained', 'coarse-grained' and 'water-saturated sand' sediments. Fine-grained sediments include a mixture of water and clay and silt size particles, coarse-grained sediments include a mix of water and clay, silt and sand size particles and water-saturated sand sediments include a mix of water and sand particles. For a given solids concentration, the content of fine particles in these sediments influences their overall bulk density. As indicated earlier, fine-grained sediments are usually the least dense, followed by coarse-grained sediments and finally water-saturated sand sediments. The rheological behaviours of each type of sediment are discussed in turn below.

The multiphase nature of sediments results in solid-solid, solid-fluid and electrostatic interactions that combine to cause complicated non-Newtonian rheological behaviours such as viscoplasticity, unsteady gravitational flow, thixotropy, and liquefaction (Takahashi 1991; Iverson 1997). Thixotropy involves the agitation or shearing of an aggregate of clay particles, which disturbs the interactions of their electrostatic potentials and leads to a temporary decrease in both the apparent yield stress and viscosity of the bulk material.

Sediments containing larger coarse-grained particles are subject to liquefaction, a process similar in effect to thixotropy. Many liquefaction mechanisms have been described and different accounts of the physics involved have been given (Allen 1985; Owen 1987; Maltman 1994; Nichols 1995). The consensus between all the different explanations is that the solid matrix of coarse-grained particles – which in this case exists due to intergranular friction rather than electrostatic interactions – is temporarily disrupted by effects such as intense vibration caused by earthquakes or increases in pore fluid pressure above hydrostatic values. However, for the purposes of this study it is enough to know that the action of a liquefaction mechanism results in a sudden loss of strength of the sediment.

Geologists commonly view reverse-density features such as flame structures in sands as having involved some degree of liquefaction, for example through the sediment having been disturbed seismically. Experiments on geological materials seem to support this inference (e.g. Anketell *et al.* 1970). Thus the gravity structures are taken to have developed in a stratified soft sediment that was initially at rest metastably but began to flow spontaneously, through thixotropic behaviour or liquefaction, following triggering disturbances. A liquefied state is assumed in the following numerical simulations, leading to the advantage of enabling us to ignore the apparent yield strength that would normally exist in undisturbed sediments and which would consequently tend to resist flow. Flame structures are often loosely referred to as dewatering structures. The extent to which drainage alone would generate such forms is debatable but the models reported here do not involve water loss.

Fine-grained slurries

Sedimentation tests were conducted using kaolinite clay (Harrison 1996). The significance of electro-

Table 1. *Density and solids concentrations determined for kaolinite-clay sediments*

Type of suspension	Average percentage concentration of solids by weight	Density of deposit
Kaolinite-distilled water	24.9	1230
Kaolinite-salt water	30.3	1270

static forces in determining the degree of flocculation of clay particles means that the addition of electrolytes such as salt can produce drastic changes in the physical properties of the material. For this reason, some of the experiments involved the clay being mixed with distilled water and others with salt water at a concentration of 40 grams of salt per litre of distilled water. Sedimentation tests gave approximate solids concentrations and densities of the resulting deposits.

The results displayed in Table 1 suggest that the addition of salt led to an increase in the compaction of the deposits. It should be noted that values in Table 1 are average values of the percentage concentration of solids by weight in the sediments. In reality, the concentration of solids will vary as a function of burial. However, for the purposes of this study, the average value of the solids concentration is considered sufficient to provide insights into the effects of the non-Newtonian behaviour of clay slurries in gravity driven sedimentary structures. Using the information of Table 1, fine-grained slurries of similar solids concentrations to the deposited sediments were produced for rheological analysis. The aim of these experiments was to produce a simple rheological equation that could relate viscosity to shear rate and concentration of solids. Experiments were performed using a Carrimed Constant Stress Rheometer.

Eq. 3, the power-law model, was found to give a good fit to the test data. Within the concentration range considered for a given shear rate, increases in concentration of solids caused an exponential increase in the slurry viscosities, in agreement with previous work (e.g. Coussot & Piau 1994). The sensitivity of this relationship depended on the type of clay under consideration. Hence, the dependence of the slurry viscosities on concentration and shear rate was fitted using an equation of the form

$$\eta = (Ae^{BC})\cdot(\dot{\gamma})^{(n-1)}, \qquad (13)$$

where η is the viscosity and is given here as a function of the shear rate, $\dot{\gamma}$, rather than the second invariant of the rate of deformation tensor in order to reflect the viscometric nature of the measurements.

Table 2. *Parameters of Equation (13) determined from equations fitted to rheological tests on kaolinite-clay sediment*

Type of slurry	A (Pa.s^n)	B	n
Kaolinite-distilled water	0.129	0.101	0.29
Kaolinite-salt water	0.111	0.085	0.37

A is the consistency factor (Pa.s^n), B is a dimensionless constant, C is the concentration of solids in the mixture expressed as a percentage of the total weight and n is the power-law index which determines the shear-rate exponent of the slurry.

The temperature dependency for each slurry was found to be negligible between the range of 5 to 25°C. Table 2 shows the values of A, B and n determined for the kaolinite-clay slurries. These values were determined at solids concentrations ranging between 1 to 1.5 times the solids concentrations found for the deposited sediments of the sedimentation tests. This range was chosen for analysis since preliminary experiments (Harrison 1996) suggested the small-scale sedimentary structures investigated here are much more likely to flow while the sediments contain high water contents and offer little resistance to deformation. As a result of these experiments, the power law model was chosen to approximate the behaviour of fine-grained sediments in the numerical simulations.

Coarse-grained slurries and water saturated sand

Attempts to derive simple equations that relate the concentration of solids to the relative viscosity between the liquefied dispersion and the interstitial fluid have been reviewed by Allen (1984). While these theories provide estimates for the viscosity of liquefied sand of the order 0.1 to 1 Pas, they fail to include shear rate dependence of the viscosity. Furthermore, experimental observation of asynchronously varying stresses in the solid and fluid phases of debris flows suggests the complex interaction between granular temperature and pore fluid pressure necessitates the use of two-phase models in explaining the behaviour of coarse-grained slurries (Iverson 1997). Even so, having drawn attention to the difficulties in modelling the flow behaviour of large-grained slurries, we point out that in using the numerical code, we are currently restricted to choosing well-defined one-phase rheological models.

Attempts to study the rheological behaviour of coarse-grained slurries experimentally have prompted various techniques, such as experiments using large-scale rotational rheometers capable of

accommodating large particle size, or alternatively, velocity measurements of debris flowing down inclined channels. However, the difficulties in investigating the precise behaviour of particulate flows are often reflected by the ambiguity of flow curve data (e.g. Phillips & Davies 1989; Holmes *et al.* 1990).

In general, therefore, while results presented in a previous section point clearly to the use of the power-law model in describing the behaviour of the lower layer of fine-grained sediment, the choice for the upper layer is less obvious. As indicated earlier, both the upper and lower layers of the instabilities considered here are presumed liquefied by a triggering disturbance before the onset of flow. This means that cohesive and intergranular frictional strengths are ideally reduced to zero. Consequently, terms representing sediment strength in rheological models such as the one presented by Johnson & Martosudarmo (1997) vanish. The effects of pore fluid rheology and intergranular collisions then govern the behaviour. Each of these, according to theory, can have non-linear dependencies on the shear rate. However, flow-data following yield can often be fitted equally well by linear or non-linear flow curves. In particular, linear fitting becomes increasingly plausible for sand-water mixtures of decreasing solids concentration (e.g. see data presented in Johnson & Martosudarmo 1997). Although in doing so, factors such as the 'dispersion gap' (Johnson 1984) and the strong dependence of viscosity on solids concentrations (Allen 1984) must be neglected. As an approximation then, both power-law and Newtonian behaviour might be used in modelling the behaviour of fully liquefied coarse-grained and sand-water sediments. Use of these simple rheological models in approximating the behaviour of natural sediments, although distancing the simulations from the details of the real situation, facilitate the use of numerical models as a first step in investigating the effects of non-linear rheological behaviour in the lower or possibly both sediment layers.

Investigating the form of the deforming interface using the numerical code

In this section, we use the code to investigate factors that could possibly influence the form of the interface between the layers and consequently the form of resulting sedimentary structures. The factors considered are the:

- size and form of the initiating perturbation;
- effects of inertial flow;
- introduction of a power-law rheological model.

Each of these factors is indeed found to influence the form of the rising intrusion. In particular, these factors are found to be conducive to the formation of a more pointed or cuspate intrusion form for the rising lower layer. Note that for all the simulations of this investigation, a very low value for the surface tension coefficient for all fluids was used (10^{-7} Nm^{-1}). Thus, the results and conclusions of the work apply only to systems in which surface tension between the fluid interfaces plays a negligible role. Since all the geological materials modelled here are all water based, they are presumed to have similar surface tension coefficients, consequently surface tension should have little effect at the fluid-fluid interfaces.

Effect of initiating perturbation

Theoretically, if two fluid layers of differing densities are arranged with the layer of greater density on top, they can remain in this meta-stable state for an indefinite period of time. Thus, in order to initiate flow, a perturbation must be introduced into the system. For the purposes of analytical theory, a periodic sinusoidal interface between the fluid layers is often used as the starting perturbation of the instability (e.g. Ramberg 1981; Johnson & Fletcher 1994). Other experimental, theoretical and numerical investigations have incorporated more localised perturbations in which second generation structures develop due to the disturbance provided by the growth of primary structures (e.g. Parker & McDowell 1955; Woidt 1978). Kelling & Walton (1957) postulated that reverse-density structures in natural submarine sediments are often initiated at water current marks on the seafloor, which would often tend to have a localised, discontinuous form. With this in mind, results of simulations presented in this section were initiated by small, localized perturbations of an otherwise flat interface.

An investigation into the influence of the initiating perturbation, on the wavelength that eventually dominates the flow pattern of a system, has been performed previously (Schmeling 1988). The results suggested that under certain circumstances, the characteristic wavelength predicted by analytical theory is not necessarily the one that dominates the mature flow pattern. In this section, we show that the size of a localized disturbance can have profound effects on the subsequent form of a rising intrusion.

Figure 2 shows the development of a fluid dome inside a cylindrical geometry. The simulations incorporated a no-slip condition on the walls of the container and an axis of rotation about which the domain was rotated. Thus, the simulation is a two-dimensional mathematical problem but shows the rise of a dome in three-dimensional Cartesian space. The only difference between the two simulations of Figure 2 was the shape and size of the initial pertur-

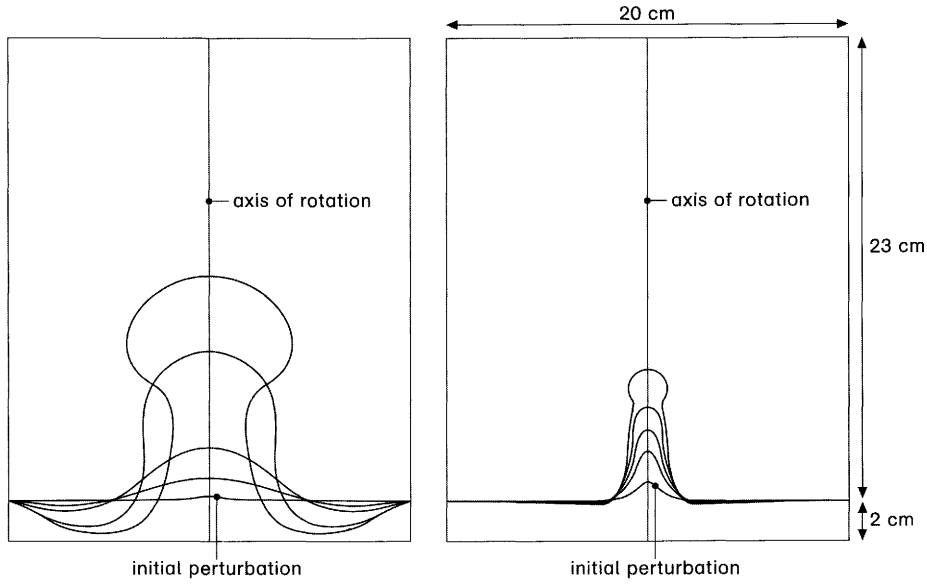

Fig. 2. Effect of perturbation size: axisymmetric simulation with rotational symmetry. Domes forming in rising fluid from small (left-hand side) and large (right-hand side) interfacial perturbations. Cylindrical geometry measuring 20 cm diameter and 25 cm high. Both the upper and lower fluids are Newtonian and of viscosity equal to 0.1 Pas. The form of the interface is shown at progressive stages in the evolution of the domes.

bation. The influence of the perturbation is dramatic and totally alters the form of the rising intrusion. This result is explored in subsequent simulations.

Effects of inertial flow

As discussed earlier, disturbed sediments may temporarily possess relatively low viscosities and thus provide scope for inertial flow during their deformation. Graphical comparisons have been drawn by Ramberg (1981) between the predictions of his own non-inertial theory and Chandrasekhar's (1955) inertial theory. These comparisons show how the predictions of the two theories diverge as inertial flow becomes increasingly important. In particular, they demonstrate how Chandrasekhar's (1955) inertial theory predicts a smaller wavelength for the flow pattern than the prediction made by Ramberg's non-inertial theory, for identical systems in which inertial terms in the analytical equations are large enough to be considered significant.

In this section, the effects of inertial flow on the flow patterns of instabilities initiated from localised perturbations are investigated. In order to do so, a series of four numerical simulations was conducted in which the effects of inertia in each successive simulation were increased. The Reynolds number (e.g. Turcotte & Schubert 1982) provides a ratio between inertial and viscous forces during flow

$$R_N = \frac{v\rho L}{\eta} \tag{14}$$

where R_N is the Reynolds number, v is the velocity of flow, L is the characteristic length of the system, ρ is the density of the fluid and η is the dynamic viscosity of the fluid. Increasing values of R_N indicate an increasing influence of inertia in relation to viscosity. Thus, by increasing the density of the upper fluid layer in a reverse-density system, R_N is increased, not only because of the increase in ρ of the upper fluid, but also because of the subsequent increase in v which is a direct consequence of the greater buoyancy forces in the system. (The complex flow, involving two fluids and both spatially and temporally changing shear rates means that it is difficult to give actual values for R_N. However, using the depth of the fluids for L and the rate of rise for v, we give a very rough estimate of R_N in the order of 10^1-10^2 for the upper fluid in the final simulation of Figure 3. The effects of inertia are investigated by comparing simulations in which inertial effects are altered).

Figure 3 and all subsequent simulations are two-dimensional planar simulations. In each figure, the simulations mirror image in the plane of symmetry is shown in order to better illustrate the form of the rising intrusions. Figure 3 clearly demonstrates how increasing the importance of inertia results in a decrease in the wavelength of the flow pattern within

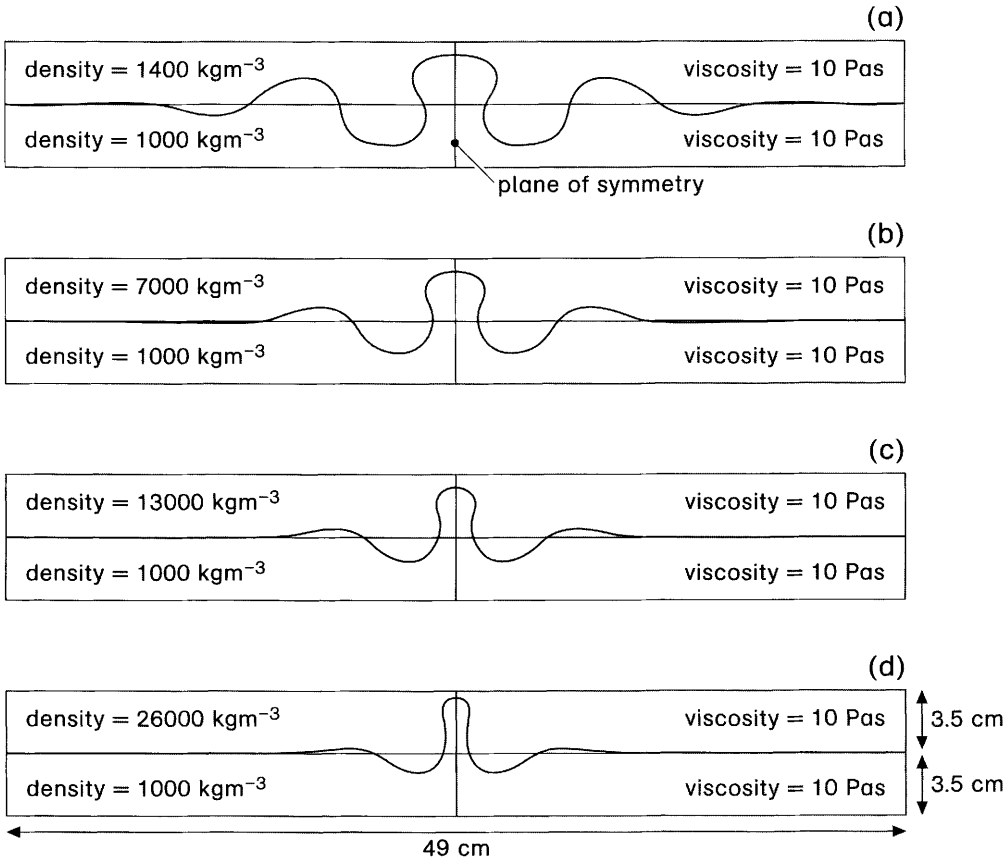

Fig. 3. Effect of inertia: viscosities and densities are shown in the figure. A no-slip boundary condition was used on three sides of the geometry along with a moving interface condition and the vertical plane of symmetry. The diagrams show the initial form of the interface, along with its shape at later stages of development.

the system and that the form of the rising structure is seen to decrease in width. Also evident is the fact that the rate of lateral progress of the flow pattern, in relation to the vertical growth of the perturbation, decreases as inertia becomes more important. This latter observation has implications regarding the form of reverse-density sedimentary structures that are created as a result of inertial flow and are initiated from localised perturbations. As inertial flow becomes more important in their genesis, these structures will tend to be more mature in relation to neighbouring structures and will become progressively more intrusive. Thus, as with the effects of the initiating perturbation, the influence of inertial flow on the form of mature rising intrusions is significant. These two results highlight the need for caution when estimating the relative viscosities of fluid layers through observations of the form of mature rising intrusive structures (Anketell *et al.* 1970; Whitehead & Luther 1975; Ramberg 1981; Jackson & Talbot 1986).

Incorporating the power-law model into the numerical simulations

In light of the previous discussion on the rheology of natural sediments, the simulations that follow use the power law model to simulate the flow behaviour of the fine-grained lower layer and either the Newtonian or power law models to simulate the behaviour of the coarse-grained upper layer. Figure 4 shows an attempt to determine the maximum value of n, the measure of shear thinning, which could be incorporated in the simulations. A two-dimensional planar geometry with a free-surface condition imposed at the upper boundary of each system was used, with planar symmetry on the left side and no-slip conditions on other outer boundaries of the geometry. The value of Ae^{BC} of Eq. (14) was chosen as 1.6 Pas^n, which corresponds to the solids concentration of a kaolinite-distilled water deposit (see Tables 1 and 2). The value of n in Eq. (14) was then decreased from a value of 1 (the Newtonian model) towards 0. The

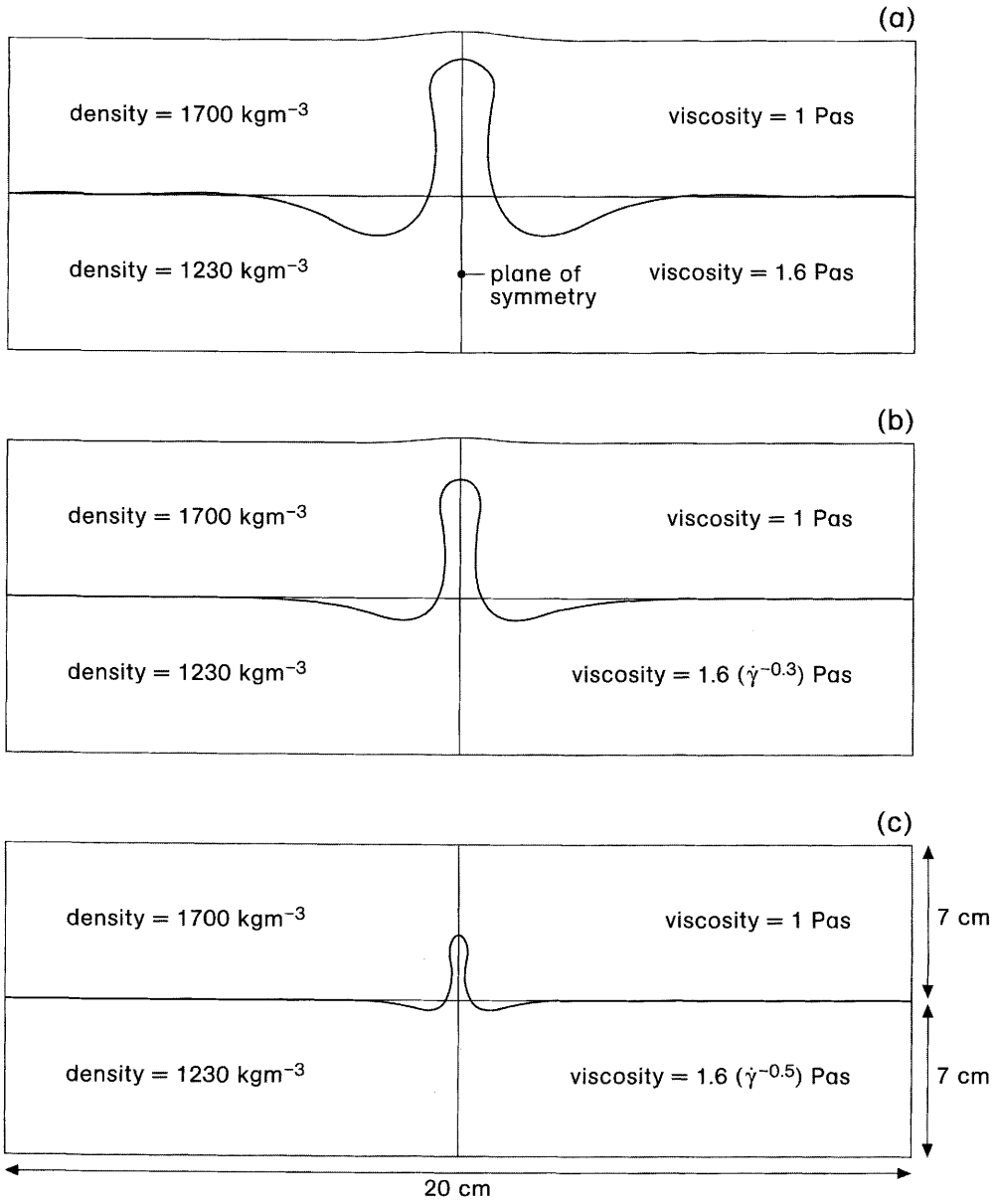

Fig. 4. A series of three simulations (a–c) using a power-law model for the lower fluid and a Newtonian model for the upper layer. The values of material parameters are shown in the figure. The depth of the layers was 7 cm.

minimum possible value of n was 0.5, hence the maximum possible degree of shear-thinning which could be incorporated in the simulations without numerical solutions calculated by the code diverging, was with a shear-thinning exponent of −0.5.

The effect of this shear thinning behaviour is apparent in Figure 4, i.e. a decrease in the wavelength of flow. Three possible reasons for this decrease are: inertial effects due to a combination of decreasing viscosity and increasing shear rates within the shear-thinning fluid; effects attributable directly to the non-linearity of the power-law model; a combination of these two factors. Estimates of the magnitude of the R_N for the three flows are more difficult to make here due to the changing viscosity and deformation rate in the lower layer. However, using a viscosity map of the lower layer, the width of the rising intrusion and the maximum rate of rise of the intrusion, rough

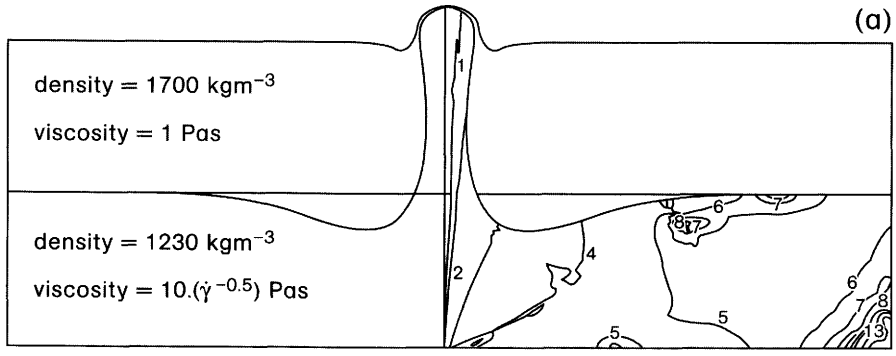

1 : 1	5 : 30	9 : 200	13 : 800
2 : 2	6 : 60	10 : 250	14 : 1000
3 : 4	7 : 100	11 : 300	15 : 1500
4 : 8	8 : 150	12 : 500	16 : 2000

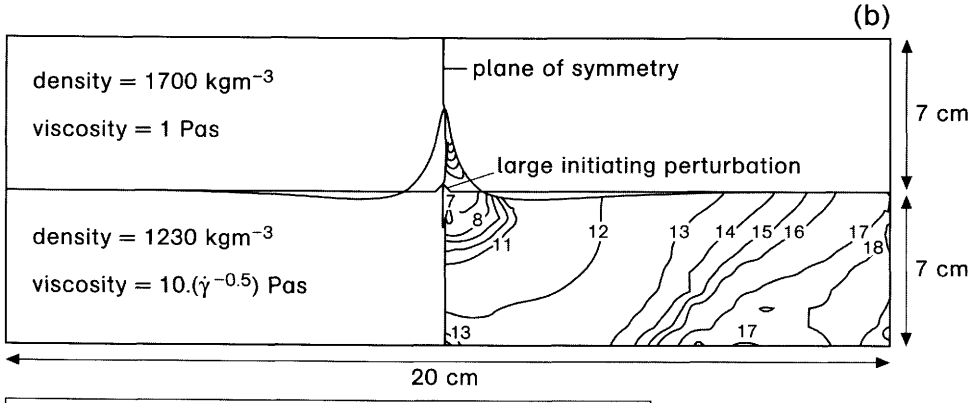

1 : 1.5	5 : 4	9 : 8	13 : 40	17 : 200
2 : 1.8	6 : 5	10 : 9	14 : 60	18 : 500
3 : 2	7 : 6	11 : 10	15 : 80	19 : 1000
4 : 3	8 : 7	12 : 20	16 : 100	20 : 2000

Fig. 5. (a) Similar simulation to Fig. 4c, but with the value of Ae^{BC} increased from 1.6 to 10 Pas. The result was an increase in the width and wavelength of the flow pattern. The duration of flow was 32.5 s. (b) Similar simulation to (a), but with the height of the initiating perturbation increased from 0.1 to 0.3 cm. The result is a dramatic change in the form of the rising intrusion. The duration of flow was 10.6 s. Viscosity maps of the lower shear-thinning fluid are superposed on the right side of the diagrams.

estimates of between 0.1 to 10 were made for R_N of the lower layer of Figure 4 (a–c). From this range of R_N it is difficult to say whether or not the decreasing wavelength was indeed due to inertial effects. Thus, to determine the reason for the decrease in wavelength in Figure 4 further simulations were conducted.

The value of Ae^{BC} in the lower layer was increased from 1.6 to 10 Pas^n, holding n at 0.5. Thus, the viscosity of the lower power-law fluid was increased. Any possible influence of inertia was consequently decreased without altering the non-linearity introduced by the power-law model. The result is shown in Figure 5(a).

Figure 5 shows that the width of the rising intrusion increases with respect to that of Figure 4c. For non-inertial flow of Newtonian fluids, if one increases the viscosity of the lower layer relative to the upper layer, one expects to see the formation of

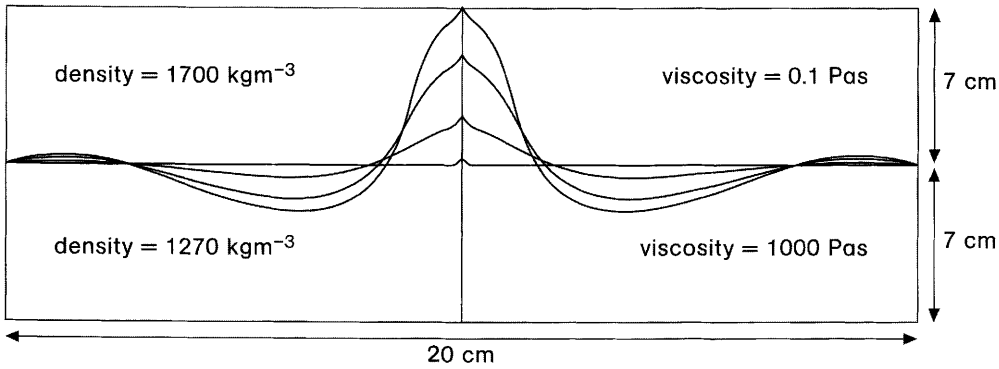

Fig. 6. Simulation in which both fluids are Newtonian. The material parameters are shown in the figure. The depth of each layer is 7 cm. The initiating perturbation was 0.3 cm high with a total width of 0.8 cm. The form of the interface between the fluids is plotted at various stages in the evolution of the instability; the final stage was achieved after 125 s. Even with this large perturbation the rising intrusion failed to adopt the cuspate form.

an increasingly narrow rising intrusion. This is not observed in the simulations of Figure 4c and Figure 5a; in fact, the opposite is observed.

Certainly, the increased viscosity of Figure 5a relative to Figure 4c means that inertia must play a smaller role in the simulation of Figure 5a than in Figure 4c. In addition, since increasing inertial flow was previously found to decrease the wavelength and width of rising intrusions, the results of the simulations suggest that inertial flow was indeed the mechanism behind the decreasing wavelength in Figure 4 (a–c). Furthermore, since the simulations of Figure 5 included viscosities comparable to those expected in natural sediments, we conclude that inertia is likely to be important during the genesis of reverse-density soft sedimentary structures in nature.

Figure 5b shows a simulation in which all parameters were identical to that of Figure 5a, apart from the height of the initiating perturbation that was increased from 0.1 to 0.3 cm in height, keeping the base width of the perturbation constant at 0.6 cm. As in Figure 1, the change in the perturbation produced a dramatic change in the form of the rising intrusion. The simulation initiated using a small perturbation, Figure 5a, is rounded whereas that initiated using a large perturbation, Figure 5b is of a pointed or cuspate form, very similar to the flame structure of Figure 1. Following this result, various tests were performed to identify more precisely the reason behind the cuspate morphology of the rising intrusion.

Cuspate morphology in reverse-density soft sedimentary structures

As with previous experiments, many of the simulations have produced various bulbous forms for both the sagging load casts and the rising intrusions. However, many natural flame structures are distinctly pointed and cuspate but this form has proven particularly elusive in previous simulations. Anketell *et al.* (1970) surmised that a large viscosity ratio is probably the critical condition for generating this morphology, but even experiments that included the non-inertial flow of Newtonian fluids with an extremely large viscosity ratio have had little success in its simulation (Whitehead & Luther 1975). In the present work, the factors considered in the attempt to determine the conditions necessary for the creation of the cuspate morphology were:

- viscosity of the upper and lower fluids and the ratio between them;
- size of the initiating perturbation in the system;
- inertial flow of the fluids;
- shear thinning fluid behaviour.

Viscosity ratio

Numerical simulations were carried out on Newtonian fluids with various viscosities and ratios as high as 10000 and in no instance did the rising structure develop a cuspate morphology (e.g. Fig. 6). Thus it is evident that a high viscosity ratio is not on its own, capable of producing a cuspate structure. The experiments were conducted with both small and large perturbations but these also failed to provide appropriate conditions for cuspate structures to form in these Newtonian fluids.

Inertial flow

The only experiment we know of that has produced cuspate morphologies in Newtonian fluids is that

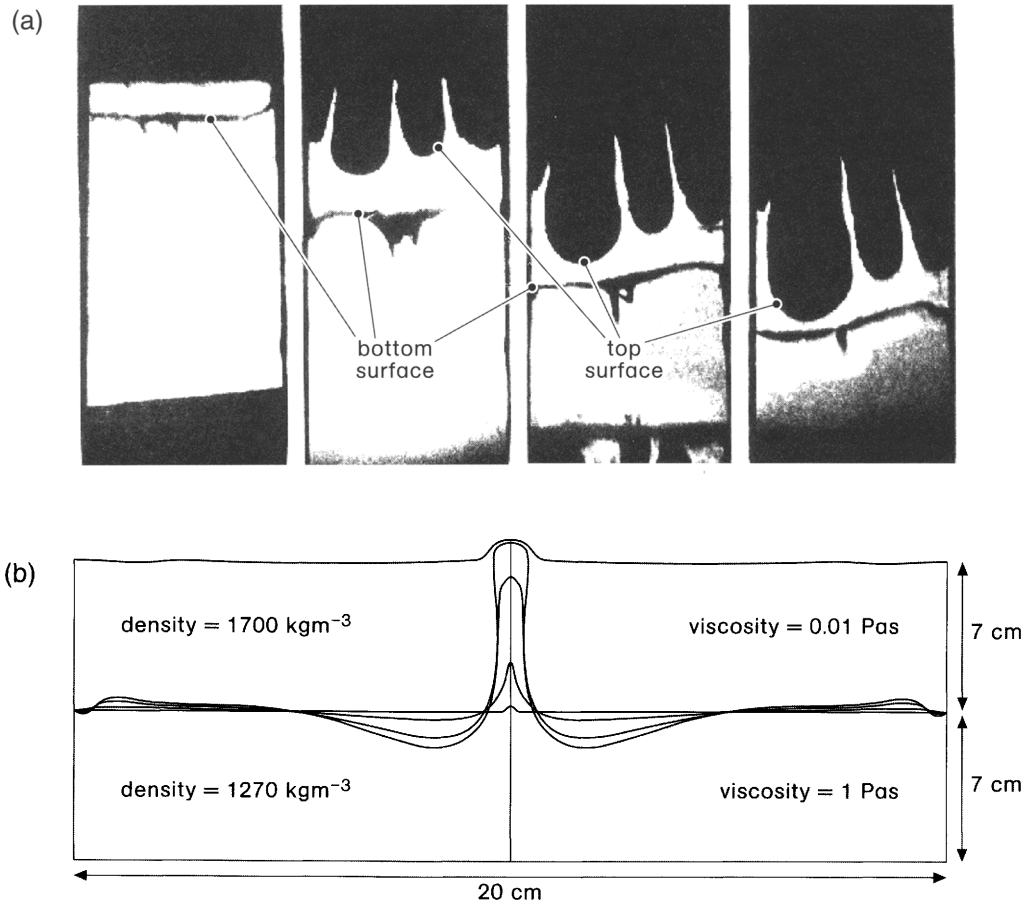

Fig. 7. (a) Photograph from the experiment conducted by Lewis (1950). The result was unusual in that the fluids used in the experiment were Newtonian and yet the form of the rising intrusions was cuspate. The depth, length and width of the water layer was 2.8, 6.25 and 1.25 cm respectively. We infer that the cause of the cuspate form is the non-linear influence of the inertia-dominated flow. (b) Simulation of a system containing Newtonian fluids in which inertia plays an important role during the flow. The depth of each layer is 7 cm. The form of the rising intrusion is cuspate during the early stages of its evolution. Material parameters are shown in the figure. The time taken to reach the last stage of deformation was 0.6 s.

conducted by Lewis (1950) (Fig. 7a). This experiment was originally conceived to verify the linear inviscid analysis proposed by Taylor (1950). It is inferred from the speed of the experiment that it involved significant inertial flow. The experiment used fluids of low viscosities, namely air and water, initially stratified in a stable configuration. The interface was of approximately sinusoidal form, due to a standing wave on the surface of the water. The fluids were rapidly accelerated downwards so that they experienced approximately 21g and flowed extremely quickly: the photographs recording the flow were separated by only milliseconds. These high speeds acting on fluids of low viscosities mean that inertia must have played a dominant role during the flow (see Eq. 14). Consequently, in order to increase the influence of inertia in this study's simulations were carried out using low viscosity Newtonian fluids for both layers. The result, shown in Fig. 7b, was partially successful in that the rising intrusion assumed a cuspate form during the early stages of flow, although it tended towards a more rounded structure during the later stages. The results indicate that non-linear effects due to inertial flow do indeed play a role in producing pointed forms.

We continued the investigation of the cuspate form by considering the effects of non-Newtonian behaviour. Numerical simulations similar to that shown in Figure 5b, but which incorporated the same power-law model in both the upper and lower layers,

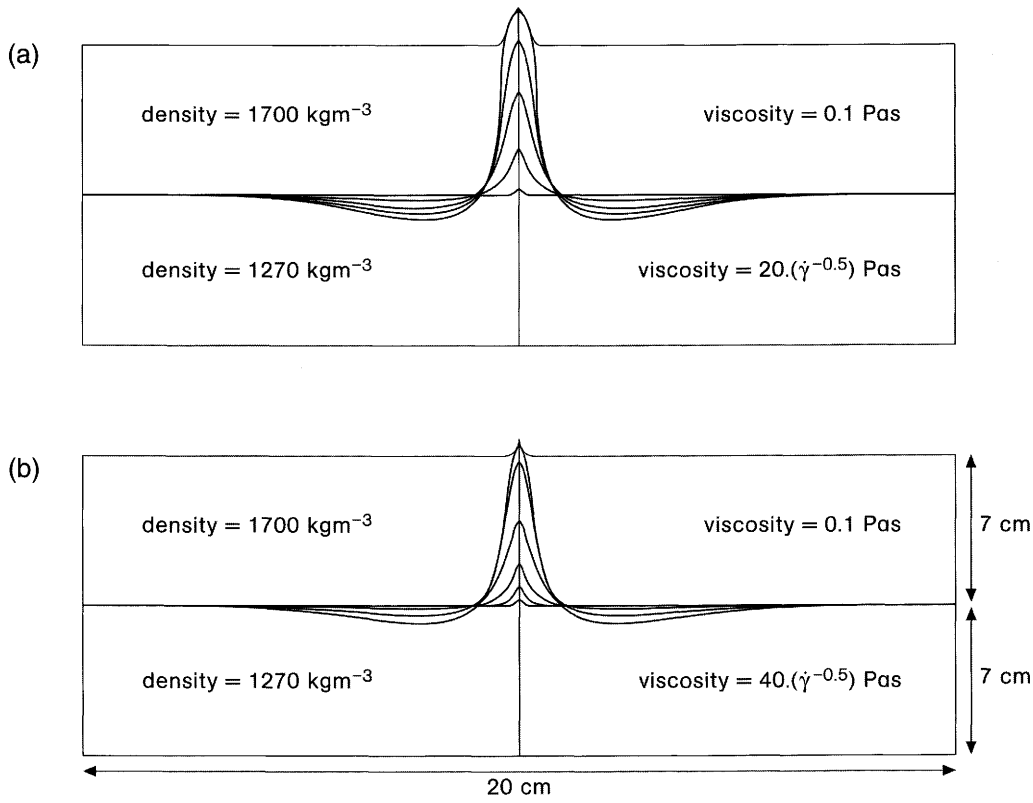

Fig. 8. (a) Simulation of a shear-thinning fluid rising through a Newtonian fluid. Material parameters are shown in the figure. The interface between the two fluids is shown at progressive stages in the evolution of the flow pattern. The time taken to reach the last stage was 27 s. (b) Same parameters as (a) but with $Ae^{BC} = 40$ Pas^n. The time taken to reach the latest stage of the evolution was 105 s. The morphology of the rising intrusion is seen to be more cuspate than that in (a).

completely failed to produce a cuspate morphology. Two further simulations were conducted similar to Figure 5b, but with differing viscosity ratios between a Newtonian fluid in the upper layer and a power-law fluid in the lower layer. The size of the initiating perturbation and the viscosity of the upper layer was held constant in each simulation, but the viscosity of the lower, power-law, fluid was increased by changing the value of Ae^{BC} in Figure 8a to 20 Pas^n and in Figure 8b to 40 Pas^n. Here, pointed morphologies did result and the rising intrusion became increasingly cuspate as the viscosity of the shear-thinning fluid was increased.

Although the simulations that involved low-viscosity Newtonian fluids for both layers suggested that inertial flow helped promote a cuspate morphology, the increase in viscosity of the lower layer of Figure 8b means that the importance of inertia is smaller relative to the simulation of Figure 8a. Thus, it is inferred that the influence of inertial flow is not itself the cause of the increasingly cuspate forms of Figure 8a and b. This investigation has also illustrated how extremely high viscosity ratios between Newtonian fluid layers fail to produce a cuspate morphology. Thus, neither can the increasing viscosity ratio between the fluid-layers fully account for the increasingly cuspate forms of Figure 8. The only other possible factor is the non-linear influence of the lower layer. It is concluded, therefore, that in Figure 8 it is the non-linear power-law behaviour of the lower layer that is particularly conducive to the production of a cuspate morphology. In addition, the greater the viscosity ratio between the lower, shear thinning fluid and the upper fluid, then the more attenuated is the form of the rising intrusion. It should be noted that all the simulations that produced a pointed intrusion, required a relatively large initiating perturbation.

Discussion

The simulations reported in the previous sections provide insights into the various influences on flow patterns and the resulting structures in geological sediments with reverse-density stratification.

Although bulbous forms are produced under a range of conditions, we have demonstrated that under certain circumstances cuspate morphologies in rising intrusions are favoured. In particular, two possible explanations have been identified. The first is a non-linear effect caused by significant inertial flow and occurs whenever the viscosities of the fluid layers are sufficiently low or when the density contrast between the fluid layers is sufficiently high. The second is also a non-linear effect due to non-Newtonian fluid behaviour in the lower layer. In this case, it is a high viscosity ratio between the lower and upper fluid layers that is conducive to the formation of the pointed morphology.

How likely are these various conditions in natural systems? Geological sediments are deposited with a range of densities and it is well known that they can exhibit non-Newtonian behaviour and undergo liquefaction processes, which allow inertial flow and induce temporary reductions in apparent yield strength. Given these reasonably common situations, acting in conjunction with the relatively large surface perturbations that readily form during the deposition of sediment layers in dynamic, subaqueous environments, all the conditions identified in our investigation are perfectly possible in nature for the production of cuspate morphologies.

Of the two means thought here to be favourable for generating these forms, it is thought that the role of non-Newtonian behaviour in the lower layer is the more important in the geological setting. Although inertial flow provides a mechanism for inducing cuspate rising intrusions, it only appears to operate, with instabilities containing Newtonian fluids and small initiating perturbations, under artificially high accelerations unlikely during the flow of natural sediments that are driven purely by buoyancy forces. In the simulation that used the inertial mechanism to produce a cuspate form of the rising intrusion, Figure 5b, a relatively large initiating perturbation was a necessary additional condition. However, a recently deposited fine-grained sediment of low solids concentration, and consequently low viscosity and insignificant apparent yield strength, would seem unable to support such a large perturbation on its upper surface during burial.

The following scenario is, therefore, envisaged, involving non-linear flow of the lower layer, for the production of the cuspate morphology. A fine-grained sediment is deposited and left undisturbed for a period of time, during which it undergoes self-weight consolidation. The sediment's viscosity increases exponentially with the increasing solids content and eventually a small apparent yield strength develops, sufficient to allow any scours or other irregularities that develop on the sediment surface to be preserved. Ensuing deposition of a coarse-grained layer takes place; once settled its density is immediately greater than the lower fine-grained clayey layer and effectively creates a Rayleigh-Taylor instability. The two layers stay in this reverse-density stratification until the onset of some liquefying mechanism. If the self-consolidation process continues for a sufficiently long period before the deposition of a denser layer, or if lithification of the layers becomes significant before any liquefaction, then the sediments remain in this metastable state without undergoing deformation. The layers become preserved in the sedimentary record without reverse-density structures ever having been initiated. However, if some disturbance occurs while the metastable sediments are still susceptible to liquefaction or thixotropic behaviour, the apparent yield strengths of both the upper and lower sediments are drastically reduced and the interfacial irregularities preserved on the upper surface of the lower fine-grained layer behave as the relatively large initiating perturbations necessary for the production of a cuspate morphology. While the lower layer flows in a non-linear shear-thinning manner, the low packing efficiency of the recently deposited coarse-grained upper sediment layer is conducive to low-viscosity Newtonian flow. The simulations of our experiments suggest that the flow of the sediments occurs probably over a time-scale of seconds. Since initiating irregularities will vary in size in nature, the requirement of a large, localised initiating perturbation in creating a cuspate morphology may explain why reverse-density soft sedimentary structures of different morphologies can develop side by side, as in Figure 1, with only some of the structures developing a cuspate form.

Finally, during liquefaction and deformation of the sediments, the packing efficiency of the upper sand and water or coarse-grained sediment increases. Thus, upon restoration of grain contacts, the sediment's apparent yield stress is significantly increased. Consequently, the likelihood of further liquefaction and deformation of the sediments is immediately reduced. Continuing sedimentation, burial and lithification progressively increase the strength of the materials, eventually precluding further flow altogether. Ultimately, lithification becomes complete and the reverse-density structures are preserved in the sedimentary record.

This work would not have been possible without the help and support of Professor K. Walters. The expertise of V. Navez and E. Degand in using the Polyflow numerical code was also invaluable. C. Talbot and R.A. Hindmarsh provided helpful comments on the manuscript.

References

ALLEN, J.R.L. 1984. *Sedimentary Structures: Their Character and Physical Basis, volumes I and II.* Elsevier, Amsterdam.

ALLEN, J.R.L. 1985. *Principles of Physical Sedimentology*. George Allen and Unwin, London.

ANKETELL, J.M. & DŻUŁYŃSKI, S. 1968. Patterns of density controlled convolutions involving statistically homogeneous and heterogeneous layers. *Annals of the Geological Society of Poland*, **38**, 401–409.

ANKETELL J.M., CEGLA, J. & DŻUŁYŃSKI, S. 1970. On the deformational structures in systems with reversed density gradients, *Annals of the Geology Society Poland*, **40**, 3–30.

BIOT, M.A. & ODÉ, H. 1965. Theory of gravity instability with variable overburden and compaction. *Geophysics*, **30**, 213–227.

BIOT, M.A. 1963*a*. Theory of stability of multi-layered continua in finite anisotropic elasticity. *Journal of the Franklin Institute*, **276**, 128–153.

BIOT, M.A. 1963*b*. Stability of multi-layered continua including the effect of gravity and viscoelasticity. *Journal of the Franklin Institute*, **276**, 231–252.

BRODZIKOWSKI, K. & VAN LOON A.J. 1985. Inventory of deformational structures as a tool for unravelling the Quaternary geology of glaciated areas, *Borea*, **14**, 175–188.

BRODZIKOWSKI, K., KRYSZKOWSKI, D & VAN LOON, A.J. 1987. Endogenic processes as a cause of penecontemporaneous soft-sediment deformations in the fluviolacustrine Czyzow Series Kleszcow Graben, central Poland). *In:* JONES, M.E. & PRESTON, R.M.F. (eds) *Deformation of sediments and sedimentary rocks*, Geological Society, London Special Publications, **29,** 269–278.

CEGLA, J., BRODZIKOWSKI, K., KIDA, J, & MORAWSKI, S. 1987. Penecontemporaneous deformation of structures formed within some fine grained Quaternary sediments (Dalkowskie Hills S.W. Poland), *Bulletin of the Polish Academy of Science*, **35**, 221–234.

CHANDRASEKHAR, S. 1955. The character of the equilibrium of an incompressible heavy viscous fluid of variable density. *Proceedings of the Cambridge Philosophical Society*, **51**, 162–178.

CHENG, D.C.H. 1987. Thixotropy. *International Journal of Cosmetics Science*, **9**, 151–191.

COLLINSON, J.D & THOMPSON, D.B. 1987. *Sedimentary Structures*, 2nd edition. Chapman and Hall, London.

COUSSOT, P. & PIAU, J.M. 1994. On the behaviour of fine mud suspensions. *Rheologica Acta* **33**, 175–184.

DEBBAUT, B., AVALOSSE, T., DOOLEY, J. & HUGHES, K. 1997. On the development of secondary motions in straight channels induced by the second normal stress difference: experiments and simulations. *Journal of Non-Newtonian Fluid Mechanics*, **69**, 255–271.

HARRISON, P. 1996. *Rheological and numerical modelling of reverse-density structures*. Ph.D. thesis, University of Wales, Aberystwyth, UK.

HOLMES, R.R., WESTPHAL, J.A & JOBSON, H.E. 1990. Mudflow rheology in a vertically rotating flume. *Hydraulics/Hydraulogy of Arid Lands, Proc. A.S.C.E. 1990 International Symposium*, 212–217.

IVERSON, R.M. 1997. The Physics of Debris Flows. *Reviews of Geophysics*, **35**, 245–296.

JACKSON M.P.A. & TALBOT C.J. 1986. External shapes, strain rates, and dynamics of salt structures. *Geological Society of America Bulletin*, **97**, 305–323.

JOHNSON, A.M. 1984. Debris flow. *In:* BRUNSDEN, D. & PRIOR, D.B. (eds) *Slope Instability.* John Wiley, New York, 257–361.

JOHNSON, A.M. & FLETCHER, R.C. 1994. *Folding of Viscous Layers; Mechanical Analysis and Interpretation of Structures in Deformed Rock,* Columbia University Press, New York.

JOHNSON, A.M. & MARTOSUDARMO, S.Y. 1997. Discrimination between inertial and macro-viscous flows of fine-grained debris with a rolling-sleeve viscometer. *Debris-Flow Hazards Mitigation: Mechanics, Prediction and Assessment, Proceedings of first international conference, Hyatt Regency San Francisco, San Francisco, California*, 229–238.

KELLING, G. & WALTON, E.K. 1957. Load-cast structures: Their relationship to upper-surface structures and their mode of formation. *Geological Magazine*, **44**, 481–491.

KUENEN, PH. H. 1953. Significant features of graded bedding. *Bulletin of the American Association of Petroleum Geologists*, **37**, 1044–1066.

LEWIS, D.J. 1950. The instability of liquid surfaces when accelerated in a direction perpendicular to their planes, II. *Proceedings of the Royal Society* **202**, 81–96.

MACOSKO, C.W. 1994. *Rheology: Principles, Measurements and Applications*. VCH Publishers, New York.

MALTMAN, A.J., 1984. On the term "soft-sediment deformation". *Journal of Structural Geology* **6**, 589–592.

MALTMAN, A.J. (ed.) 1994. *The Geological Deformation of Sediments.* Chapman and Hall, London.

NICHOLS, R.J. 1995. The liquefaction and remobilization of sandy sediments. *In:* HARTLEY, A.J. & PROSSER D.J. (eds) Characterization of Deep Marine Clastic Systems. Geological Society, London, Special Publications, **94**, 63–76.

OWEN, H.G. 1987. Deformation processes in unconsolidated sands. *In:* JONES, M.E. & PRESTON, R.M.F. (eds) *Deformation of sediments and sedimentary rocks*. Geological Society, London, Special Publications, **29**, 11–24.

PARKER, T.J. & MCDOWELL, A.N. 1955. Model studies of salt dome tectonics. *Bulletin of the American Association of Petroleum Geologists*, **39**, 2384–2471.

PETTIJOHN, F.J. & POTTER, P.E. 1964. *Atlas and Glossary of Primary Sedimentary Structures*. Springer-Verlag, New York.

PHILLIPS, J.P. & DAVIES, R.H. 1989. Generalised viscoplastic modelling of debris flow, *A.S.C.E. Journal of Hydraulic Engineering* **115**, 1160–1162.

POLIAKOV, A., VAN BALEN, R., PODLADCHIKOV, Y., DAUDRE, B., CLOETING, S. & TALBOT, C.J. 1993. Numerical analysis of how sedimentation and redistribution of surficial sediments affects salt diapirism. *Tectonophysics*, **226**, 199–216.

PRENTICE, J.E. 1961. Some sedimentary structures from a Weald Clay sandstone at Warnham brickworks, Horsham, Sussex. *Proceedings of the Geologists Association*, **73**, 171–185.

RAMBERG, H. 1968*a*. Fluid dynamics of layered systems in a field of gravity, a theoretical basis for certain global structures and isostatic adjustment. *Physics of the Earth and Planetary Interiors*, **1**, 63–87.

RAMBERG, H. 1968*b*. Instability of layered systems in a field of gravity. *Physics of the Earth and Planetary Interiors*, **1**, 427–474.

RAMBERG, H. 1981. *Gravity, Deformation and the Earth's Crust*, 2nd edition. Academic Press, New York.

ROMER, M. M. & NEUGEBAUER, H. J. 1991. The salt dome problem: A multilayered approach, *Journal of Geophysical Research*, **96**, B2, 2389–2396.

RONNLUND, P. 1989. Viscosity ratio estimates from natural Rayleigh-Taylor instabilities. *Terra Nova*, **1**, 344–348.

SCHMELING, H. 1988. Numerical models of Rayleigh-Taylor instabilities superimposed upon convection. *Bulletin of the Geological Institutions of the University of Uppsala*, 14, 95–109.

TAKAHASHI, T. 1991. *Debris Flow*. A.A. Balkema, Brookfield, Vt.

Talbot, C. 1977. Inclined and asymmetric upward-moving gravity structures. *Tectonophysics*, **42**, 159–181.

TAYLOR, G. 1950. The instability of liquid surfaces when accelerated in a direction perpendicular to their planes, I. *Proceedings of the Royal Society*, **201**, 192–196

THOMPSON, J.F. 1985. *Numerical Grid Generation – Foundations and Applications*. Elsevier, Amsterdam.

TURCOTTE, D.L. & SCHUBERT, C. 1992. *Geodynamics; Applications of Continuum Physics to Geological Problems*. John Wiley, New York.

VAN KEKEN, P.E., SPIERS, C.J., VAN DEN BERG, A.P & MUYZERT, E.J. 1993. The effective viscosity of rock-salt: implementation of steady-state creep laws in numerical models of salt diapirism. *Tectonophysics*, **225**, 457–476.

WALTON, E.K. 1956. Limitations of graded bedding and alternative criteria of upward sequence in the rocks of the Southern Uplands. *Transactions of the Geological Society Edinburgh*, **16**, 262–271.

WHITEHEAD, J.A. & LUTHER, D.S. 1975. Dynamics of laboratory diapir and plume models. *Journal of Geophysical Research*, **80**, 705–716.

WOIDT, W.D. 1978. Finite element calculations applied to salt dome analysis. *Tectonophysics*, **50**, 369–386.

YAO, M. & MCKINLEY G.H. 1998. Numerical simulation of extensional deformations of viscoelastic liquid bridges in filament stretching devices. *Journal of Non-Newtonian Fluid Mechanics*, **74**, 47–88.